Experimental study of single, double, and multiple electron capture in slow $^{15}N^{7+}+Ne$ collisions using recoil-ion momentum spectroscopy

Hualin Zhang,* X. Fléchard, A. Cassimi, L. Adoui, G. Cremer, F. Frémont, and D. Hennecart
Centre Interdisciplinaire de Recherche Ions-Lasers, CEA/CNRS/ISMRA/Université de Caen Basse Normandie, CIRIL/ISMRA, 6 Bd. Maréchal Juin, F-14050, Caen Cedex 4, France
(Received 5 December 2000; published 12 June 2001)

Single, double, triple, quadruple, and quintuple capture of electrons in $^{15}N^{7+}+Ne$ collision at the energy of 105 keV have been investigated using recoil-ion momentum spectroscopy. Relative cross sections, stabilization ratios, ratios between single- and multiple-electron capture, along with the branching ratios of subprocesses involved in multiple capture, have been obtained and compared with calculations by the extended classical over-barrier model [A. Niehaus, J. Phys. B **19**, 2925 (1986)] and the semiempirical scaling laws [N. Selberg *et al.*, Phys. Rev. A **54**, 4127 (1989)]. For single capture, *n* state relative populations and projectile scattering angle distributions are given. In the case of double capture, we find the autoionizing double capture dominates and populates the symmetric $N^{5+}(3l3l')$ and near-symmetric $N^{5+}(3l4l')$ state, while the true double capture mainly gives rise to $N^{5+}(2lnl')$ $(n>2)$ configurations. The relative cross sections and stabilization ratios for double electron capture are evaluated. In the more than two-electrons capture, we have obtained stabilization ratios and branching ratios of different subprocesses. The configurations populated by more than two-electron captures have been identified. Our results also show that the electron-electron correlation is important in multiple electron capture.

DOI: 10.1103/PhysRevA.64.012715 PACS number(s): 34.70.+e, 34.50.Fa

I. INTRODUCTION

The study of electron capture during ion-atom collision has undergone significant advances in recent decades [1]. On one hand, fast computers and new experimental tools, such as recoil-ion momentum spectroscopy (RIMS) [2], have greatly enhanced the scope of problems that are accessible, resulting in a level of research activities that is substantially growing. On the other hand, added incentives are provided by the importance of electron-capture processes in such diverse areas as plasmas studies, astrophysics, laser technology, biology, and materials science.

The main reason for all these exciting activities in electron capture lies in the significance of the fundamental problems that are coming within grasp. Hitherto, the understanding of single and double electron transfer has been well established [1,3,4], but the mechanisms of more than two electrons capture have, by no means, been understood. We only believe that multiple electron capture may cause electron-electron correlation effects to become strong.

To the best of our knowledge, multiple electron capture, here, namely more than two electrons transferred from target atom to projectile during the collision, is only beginning to be understood. Of those works, Posthumus and Morgenstem [5] investigated multiple-electron capture processes in collisions of Ar^{9+} on Ar by measuring the Auger electrons in coincidence with charge-state analyzed recoil ions. Through electron energy spectra, the possible configurations up to six electrons were first deduced. Ali *et al.* [6] studied multiple electron capture in 10 keV Ar^{9+} $(5<q<17)$ on Ar collisions, and they obtained absolute cross sections for total charge transfer, projectile charge change, and recoil-ion production cross sections. Araphaelian *et al.* [7], measured multiple electron capture in the $Xe^{30+}+Ar$ system at projectile velocities between 0.3 and 1.0 a.u. observing up to eight-electron capture. Martin *et al.* [8] investigated triple electron capture stabilization ratios in slow ion-atom collisions using different projectiles and target atoms. They found that double Rydberg states were populated by triple electron capture in collisions of highly charged ions with atoms. Merabet *et al.* [9] measured 60 keV $O^{7+}+Ar$ collision system to study the possible decay pathways after two- and three-electron capture. Hansen *et al.* [10] measured 28 keV $^{15}N^{7+}+Ar$, and reported evidence for significant target outer-shell excitation accompanying multiple electron capture. Emons, Hasan, and Ali [11] investigated 70 keV $^{15}N^{7+}+Ar$ collision by means of time-of-flight triple coincidence measurements, and double through quintuple capture were measured. Selberg, Bedermann, and Cederquist [12] developed semiempirical scaling laws for different electronic rearrangement features after multiple-electron capture in slow collisions with highly charged ions; This scaling law can well predict the absolute cross section for removing exactly **r** electrons from the target. They also measured multiple-electrons capture for different collision systems [13].

Using high-resolution recoil-ion momentum spectroscopy (RIMS) [14], we have measured the 105 keV $^{15}N^{7+}+Ne$ collision system concerning single capture (SC); autoionizing double capture (ADC), true double capture (TDC); triple capture followed by two-electron autoionization (C3A2), one-electron autoionization (C3A1) and true triple capture (C3A0); quadruple capture followed by three- (C4A3), two-

*Present address: Department of Physics and Astronomy, 177 Chemistry-Physics Building, University of Kentucky, Lexington, KY 40506-0055.

(C4A2), and one-electron autoionization (C4A1) and true quadruple capture (C4A0); quintuple capture followed by three- (C5A3), two- (C5A2), and one-electron autoionization (C5A1).

Due to the fact that neither experimental nor theoretical data for this system are available to be used to compare with our current experimental results, we will mainly compare our experimental data with the calculation by the extended over-the-barrier (EOB) model [15]. We also use Selberg, Biedermann, and Cederquist [12] semiempirical (SE) scaling laws to calculate the multiple capture cross section ratios, which are also used to compare with our data. The aim of this paper is to provide the detailed experimental results along with the discussion of SC, ADC, TDC, and multiple capture obtained by RIMS for the $^{15}N^{7+}+Ne$ system at the energy of 105 keV. After a brief description of the experimental setup, we will discuss our results concerning the following processes:

$$N^{7+}+Ne\rightarrow Ne^{6+}*+Ne^{+}, \quad \text{SC} \tag{1}$$

$$\begin{aligned} N^{7+}+Ne&\rightarrow N^{5+}*+Ne^{2+}\rightarrow N^{4+}+Ne^{2+}+e \quad \text{ADC}\\ &\rightarrow N^{5+}*+Ne^{2+}\rightarrow N^{5+}+Ne^{2+}+h\nu, \quad \text{TDC} \end{aligned} \tag{2}$$

$$\begin{aligned} N^{7+}+Ne&\rightarrow N^{4+}*+Ne^{3+}\rightarrow N^{6+}+Ne^{3+}+2e+h\nu \quad \text{C3A2}\\ &\rightarrow N^{4+}*+Ne^{3+}\rightarrow N^{5+}+Ne^{3+}+e+h\nu \quad \text{C3A1} \end{aligned} \tag{3}$$

$$\begin{aligned} &\rightarrow N^{4+}*+Ne^{3+}\rightarrow N^{4+}+Ne^{3+}+h\nu, \quad \text{C3A0}\\ N^{7+}+Ne&\rightarrow N^{3+}*+Ne^{4+}\rightarrow N^{6+}+Ne^{4+}+3e+h\nu \quad \text{C4A3}\\ &\rightarrow N^{3+}*+Ne^{4+}\rightarrow N^{5+}+Ne^{4+}+2e+h\nu \quad \text{C4A2}\\ &\rightarrow N^{3+}*+Ne^{4+}\rightarrow N^{4+}+Ne^{4+}+e+h\nu \quad \text{C4A1} \end{aligned} \tag{4}$$

$$\begin{aligned} &\rightarrow N^{3+}*+Ne^{4+}\rightarrow N^{3+}+Ne^{4+}+h\nu, \quad \text{C4A0}\\ N^{7+}+Ne&\rightarrow N^{2+}*+Ne^{5+}\rightarrow N^{5+}+Ne^{5+}+3e+h\nu \quad \text{C5A3}\\ &\rightarrow N^{2+}*+Ne^{5+}\rightarrow N^{4+}+Ne^{5+}+2e+h\nu \quad \text{C5A2} \end{aligned} \tag{5}$$

$$N^{2+}*+Ne^{5+}\rightarrow N^{3+}+Ne^{5+}+e+h\nu. \quad \text{C5A1}$$

We present the relative cross sections for SC, ADC, and TDC respectively, branching ratios, and stabilization ratios for more than two-electron capture. For quintuple electrons capture, due to the reason that we only recorded three possible processes, the detailed comparison is not given.

II. EXPERIMENTAL SETUP

The $^{15}N^{7+}$ projectile is provided by a 14 GHz electron cyclotron resonance (ECR) ion source of the Grand Accélérateur National D'Ions Lourds (GANIL, Caen, France) [16]. The beam is collimated by a 600 μm aperture located at the entrance of the spectrometer and two pairs of slits 3 m upstream. The ion beam crosses the target supersonic jet at the center of the spectrometer. In the first generation of RIMS, uniform electric fields were used, and the geometrical dimensions of the collision region (the overlap between the ion beam and the supersonic gas jet) [2] limited the resolution of the spectroscopy. The momentum resolution now has been improved by using a nonuniform electric field to extract the recoil ions and focuses ions with the same velocity on the position sensitive detector, whatever the starting point [14]. A field-free region follows the extraction region in order to ensure the time focusing condition [13]. Finally, the recoil ions are post accelerated toward the detector, so that the detection efficiency is independent of the charge state of the ion. After the collision, the projectile ions are charge analyzed using an electrostatic deflector associated with a second position sensitive detector. By coincidence, the scattered projectile N^{6+}, N^{5+}, N^{4+}, N^{3+}, N^{2+} with the time-of-flight of the recoil ion Ne^{1+}, Ne^{2+}, Ne^{3+}, Ne^{4+}, and Ne^{5+}, we get most of the reaction processes. For each capture event, the time-of-flight and the impact position of the recoil ion, together with the projectile position, are recorded by a list mode data acquisition. The first two quantities give direct access to the recoil-ion longitudinal $P_{R\parallel}$ and transverse $P_{R\perp}$ momentum components.

The principle of RIMS relies on the relationship between the recoil-ion momentum and two important quantities: the Q value of the reaction and the projectile scattering angle θ.

Kinetically, the capture process may be viewed as an inelastic two-body collision [2]. It is thus we can get simple relations for small scattering angles:

$$Q=-P_{R\parallel}V_p-\frac{n_cV_p^2}{2}, \tag{6}$$

$$\theta=\frac{P_{R\perp}}{P_0}. \tag{7}$$

$P_{R\parallel}(P_{R\perp})$ is the recoil-ion longitudinal (transverse) momentum. P_0 is the projectile longitudinal momentum, V_p is the velocity of projectile, and n_c is the number of captured electrons. The Q value corresponds to the potential energy released as kinetic energy and thus contains information on the state populated on the projectile by the capture process. In the particular case of N^{7+} on Ne, the resolution is high enough to separate different configurations in SC, ADC, and TDC, but it is not sufficiently high enough to separate the configurations involved in more than two-electron capture. It reached resolutions full width at half maximum (FWHM) of 10.3 eV for single capture and 14.6 eV for double capture.

Similar to our previous works [3,4], the calibration of the Q-value spectra is deduced first through the calculation results by the Landau-Zener model [17], which allows us to identify the main configurations formed in the single capture. Then, since the Q-value spectrum of single capture is made of well-separated peaks, the calibration and identification are refined using the state energies calculated by the code of Cowan [18]. The Q-value calibration for more than two-electrons capture can be easily obtained through the electrostatic relation between different recoil-ion charges, which correspond to different capture processes [2].

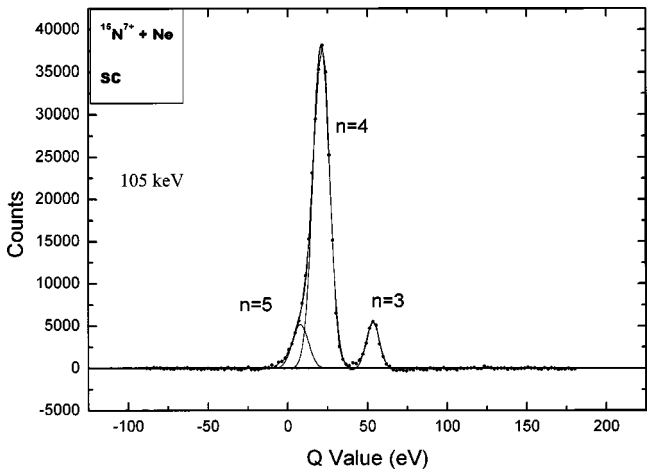

FIG. 1. Experimental single-capture Q-value spectra for the $^{15}N^{7+}$-Ne system. The different configurations ($n=3,4,5,\ldots,$) and corresponding Q values are given in Table I.

III. RESULTS AND DISCUSSION

In this part, we report experimental relative differential cross sections and partial projectile scattering angle distributions for all the recorded processes, which are single capture, double capture, and multiple captures. The relative cross sections are derived from the Q-value spectra after a fitting procedure, in which the peak shape is approximately assumed to be the Gaussian for simplicity. The errors of data in this paper originate from the fitting, efficiency correction, statistics, and background estimation [14].

A. Single-electron capture (SC)

From the SC Q-value spectrum (Fig. 1), for the different configurations (listed in Table I), the relative cross sections populated during the collision were extracted (Fig. 2). The SC Q-value spectrum and relative cross section clearly show that RIMS is able to give information not only on the configurations, but also on the relative population intensities of the terms involved in the capture process (Figs. 1,2).

In Fig. 2, we have found that the vast majority of SC events (more than 87%) take place in the N^{6+} N shell ($n=4$). M shell ($n=3$), and O shell ($n=5$) take the second and third priority, respectively.

These characteristics can be well understood from the diabatic potential curves (Fig. 3). Since N shell has a crossing with the entrance channel at the intermediate internuclear distance, while M shell has a crossing at a smaller internucleus distance, and O shell has no crossing at the intermediate internuclear distance, it would be easier to capture one electron to N shell than to capture to other shells.

TABLE I. Q values of single electron capture for the $^{15}N^{7+}+Ne$ collision.

States (n)	Q (eV)
2	145.18
3	52.54
4	20.12
5	5.40

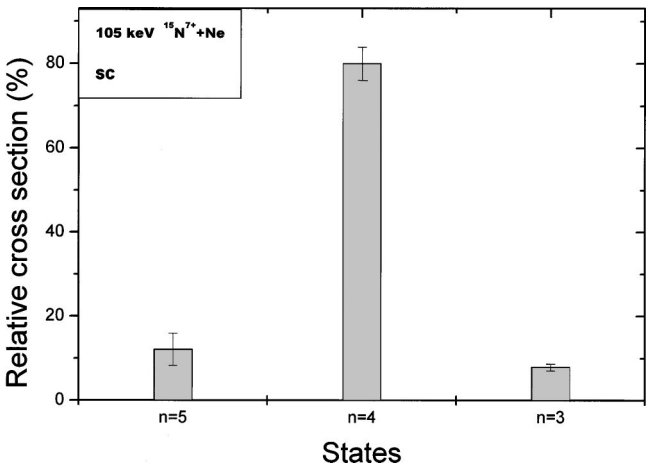

FIG. 2. Relative cross sections of SC for the $^{15}Ne^{7+}$-Ne system $\Sigma n_i=100$.

We have used the EOB [15] model to calculate the SC total cross section, as well as multiple-capture total cross sections. The ratios have been used to compare with current experimental results. The results and discussion will be given in Sec. III D.

The projectile scattering angle distributions for SC are given in Fig. 4. M-shell SC has a larger scattering angle (0.2 mrad) than $n>4$ complex terms (0.1 mrad). They can be well understood from Fig. 3, since the crossing of M shell is closer to the nucleus than N shell, the scattering angle from M shell should be larger.

B. Double-electron capture (DC)

For double-electron capture, the processes can be separated into autoionizing double capture (ADC) and true double capture (TDC).

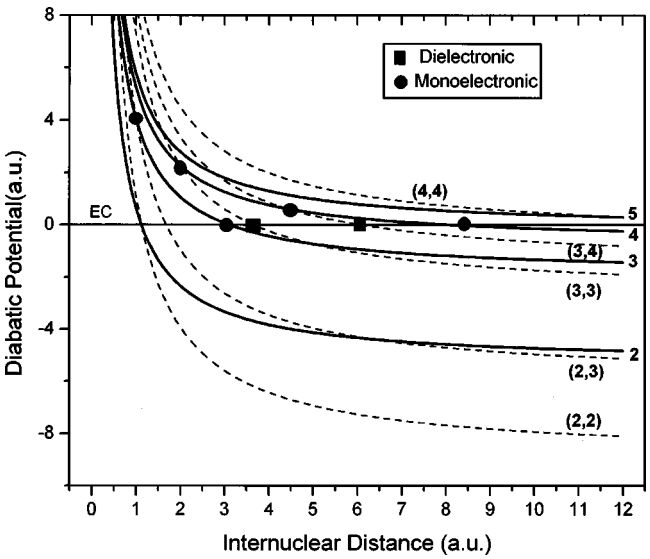

FIG. 3. Diabatic potential curves of SC and DC for the $^{15}N^{7+}$-He system. EC is Entrance Channel; 3 is the $N^{6+}(3l)$ SC channel; (3,3) is the $N^{6+}(3l3l')$ DC channel.

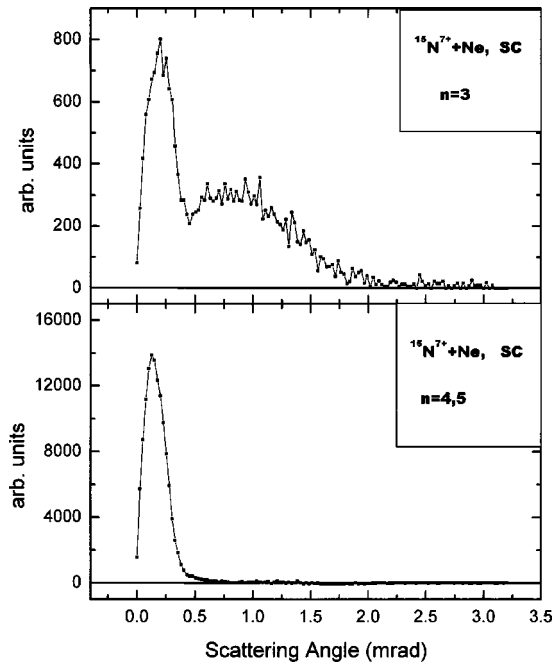

FIG. 4. Projectile scattering angle distribution of the SC $N^{6+}(3l)$ and $N^{6+}(nl,\ n\geqslant 4)$ channel.

The *Q*-value spectra for ADC and TDC are shown on Fig. 5. The calculated *Q* values corresponding to the measured states on Fig. 5 are given in Table II.

The ADC *Q*-value spectrum shows that the double-capture events mainly populate on $(3l3l')$ symmetry states (43.69%), or $(3l4l')$ near-symmetry states (25.81%). The contribution from asymmetric states $(3lnl',\ n>4)$ is about 18.69% of total ADC. $(2lnl')$ $(n>2)$ states only amount to

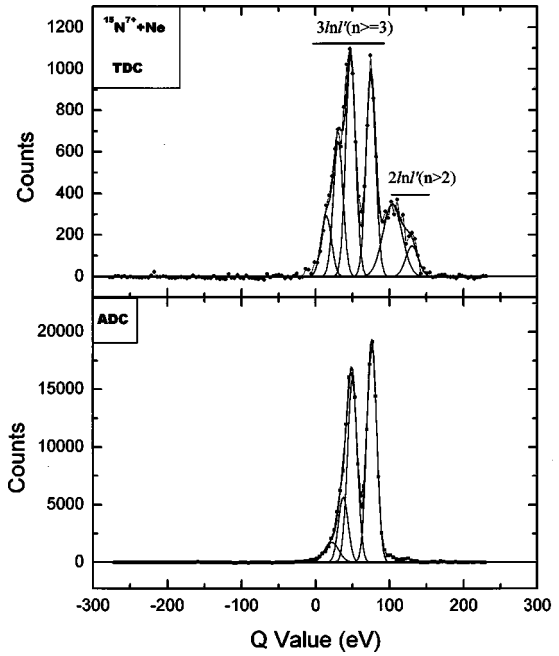

FIG. 5. Measured TDC and ADC *Q* value spectra for the $^{15}N^{7+}$-Ne system. Different configurations and corresponding *Q* values are given in Table II.

TABLE II. *Q* values of double electron capture for the $^{17}N^{7+}$+Ne collision.

Configurations	*Q* (eV)
2,2	242.92
2,3	162.01
2,4	135.91
2,5	124.09
2,6	117.89
3,3	74.14
3,4	44.47
3,5	31.97
3,6	25.48
4,4	13.73
4,5	0.41
4,6	−6.58

1.8%. The similar configurations were also found by A. A. Haasan *et al.* [10] in the 28 keV $^{15}N^{7+}$+Ar collision.

From the TDC *Q*-value spectrum, we have observed very similar configurations populated as ADC. Of all the states, $(3l3l')$ amount to 24.92% of total TDC events, $(3l4l')$ amount to 27.64%, $(3lnl')$ $(n>4)$ amount to 24.98%, and $(2lnl')$ $(n>2)$ amount to 22.46%. Therefore, the asymmetric states have larger stabilization probability than symmetry states. In all the state groups, the asymmetric state series of $(2lnl')$ $(n>3)$ has the largest stabilization ratio (52.21%). The stabilization ratios, along with the relative cross sections of ADC and TDC obtained in this experiment, are given in Table III.

Two processes may be responsible for the double capture into $(3l3l')$ configurations: a two-step process via *N*-shell $(n=4)$ SC channel at internuclear distance of about 8.4 and 2.0 a.u. (circles), or a one-step process at about 3.6 a.u. (squares) (Fig. 3). In the two-step process, one electron is first captured on the *N* shell $(n=4)$ at large internuclear distance, then this electron is excited to the *M* shell $(n=3)$ while the second electron is captured in *M* shell at smaller internuclear distance ending as bound $(3l3l')$ states. The process due to dielectronic interaction is usually called correlated transfer excitation (CTE) [19–20]. In the one-step process, the two electrons are simultaneously captured into the *M* shell at about 3.6 a.u. It is noted that this two-electron transfer, correlated double capture (CDC) is also governed by dielectronic interaction or electron-electron correlation [19]. An alternative explanation has also been proposed by Laurent *et al.* [21]. They invoked a mechanism involving a virtual transition to the SC channel at the crossing followed

TABLE III. Measured relative cross sections and stabilization ratios of double capture for 105 keV $^{15}N^{7+}$+Ne collision (%).

	$[2,\ n\ (n>2)]$	(3, 3)	(3, 4)	$[3,\ n\ (n>4)]$
ADC	1.80±0.78	43.69±1.48	35.81±1.69	18.69±2.41
TDC	22.47±2.79	24.91±1.27	27.64±1.40	24.98±2.73
Stab.	52.21±4.62	4.77±2.74	6.34±3.07	10.50±5.17

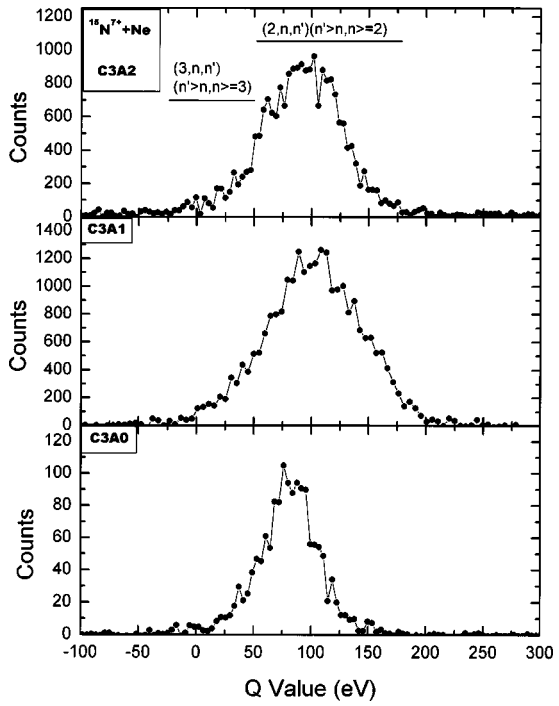

FIG. 6. Measured triple-capture Q-value spectra for the $^{15}N^{7+}$-Ne system. Different configurations and corresponding Q values are given in Table IV.

by a transition in the DC channel. Such a mechanism may be active when the SC channel is in the neighborhood of the crossing between the DC channel and the entrance channel.

Very similar to the above discussion for $(3l,3l')$, $(3l,nl')$ $(n>3)$ and $(2,n)$ $(n>2)$ may also be formed by one-step or N-shell intermediated two-step processes.

C. Triple-electron capture (C3)

With more than two active electrons, the number of channels leading to multiple capture becomes too large to be treated theoretically within the quasimolecular description using close coupling standard codes. Only the barrier model [15] and semiempirical model [12] can be used to describe these processes. Experimentally, the resolution of our spectroscopy is not high enough to separate different multiple-capture channels; Only the configurations formed by the related multiple capture could be identified.

For triple-electron capture, we have obtained the first complete set of Q-value spectra, which are true triple capture (C3A0), triple capture followed one-electron autoionization (C3A1), and triple capture followed two-electron autoionization (C3A2), respectively. Q values corresponding to the states of triple-electron capture on the spectra (Fig. 6) are given in Table IV. Because we are not able to separate the different configurations due to the limited resolution for this process, we only obtain the relative branching ratios concerning different subprocesses. Unfortunately, we have not found any theoretical results or methods for C3A0, C3A1, and C3A2, respectively, except for the total triple-capture cross section made by us using the EOB and SE models. Our experimental results of relative branching ratios show that

TABLE IV. Q values of triple electron capture for the N^{7+}+Ne collision.

Configurations	Q (eV)
2,2,3	220.6085
2,2,4	200.3199
2,2,5	191.6527
2,2,6	187.2106
2,2,7	184.5219
2,2,8	182.8655
2,2,9	181.6835
2,3,3	142.2106
2,3,4	119.4353
2,3,5	110.5012
2,3,6	105.4136
2,4,4	94.8251
2,4,5	84.6748
2,4,6	79.4993
2,5,5	74.1609
2,5,6	68.3116
2,6,6	62.6528
3,3,3	55.0515
3,3,4	31.5700
3,3,5	21.8232
3,3,6	16.9977
3,3,7	13.8513
3,4,4	4.3506
3,4,5	−6.9235
3,4,6	−11.6621

C3A0 is about 3.65%, C3A1 about 54.86%, and C3A2 about 41.49% of the total triple-electron capture. Therefore, the stabilization ratio of triple capture, here namely C3A0, is very small (3.65%).

From Fig. 6, we find that the C3A1 is the strongest subprocess in the whole C3 process. It indicates that the two electrons are most stabilized after capturing three electrons. This is because, in our observed configurations, one of three electrons is captured into either the $n=2$ or on $n=3$ shell, and the other two electrons (n and n') are captured into shells far away from this shell. So, the de-excitation of one of (n,n') can easily lead to the ionization of another electron. Of course, the de-excitation of electron on $n=2$ (or $n=3$) may lead to the ionization of two (n,n') electrons. This could explain why the branching ratio of C3A2 also is big.

Second, we find that triple capture mostly populates double Rydberg series $(2,n,n')$ or $(3,n,n')$ $(n'>n,\ n>4)$. The feature that electrons could be captured into double Rydberg states in triple capture at slow ion-atom collisions was also reported by Martin *et al.* [8].

According to the EOB model, three electrons were captured successively. But, as we will see in Sec. III D the electron-electron correlation might be a very important process in multiple capture. So, except for the three-step process in the light of the independent electron model, multielectron CTE may also be responsible for producing triple-capture states: first, one electron was captured in N-shell $(n=4)$,

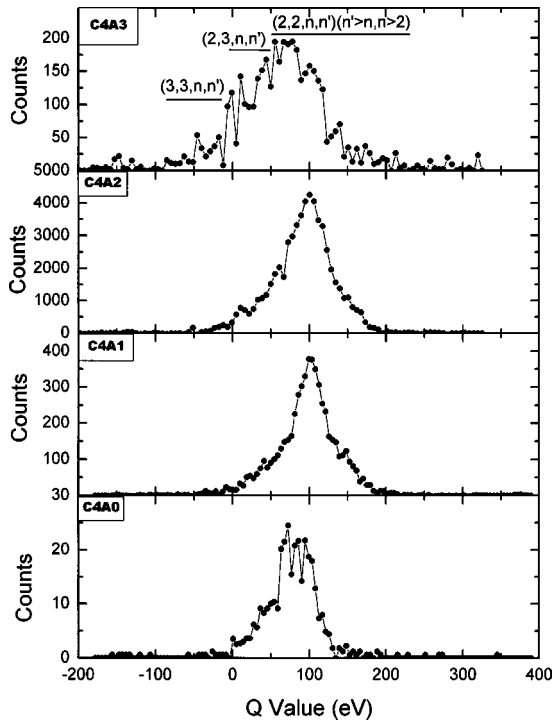

FIG. 7. Measured quadruple-capture *Q*-value spectra for the $^{15}N^{7+}$-Ne system. Different configurations and corresponding *Q* values are given in Table V.

then it was excited to the *L*-shell ($n=2$) or *M*-shell ($n=3$), while the second and third electron were simultaneously captured into Rydberg states n and n'.

In addition, from the experiment, we obtain the ratios of C3/SC and C3/DC, which are 0.18 and 0.26, respectively. They are smaller than the ratios obtained by EOB (0.31, 0.44) and by SE (0.29, 0.60). As discussed in the next section, we think that both EOB and SE models may overestimate the C3 process.

D. Quadruple-electron capture (C4)

We have separated quadruple-electron capture from other stronger processes by using the coincidence technique. Similar to triple-electron capture, we also have a complete set of data for quadruple-electron capture: They are true quadruple-electron capture (C4/A0), quadruple capture followed by one-electron autoionization (C4A1), quadruple capture followed by two-electron autoionization (C4A2), and quadruple capture followed by three-electron autoionization (C4A3). We give *Q*-value spectra (Fig. 7) and relative intensities (Fig. 8) according to how many electrons were autoionized after capturing four electrons by the projectile $^{15}N^{7+}$. The *Q* values of different configurations of Fig. 7 are given in Table V.

From the *Q*-value spectra (Fig. 7), we again find a very similar feature as that observed in the triple capture. The group of double-electron stabilization (C4A2) is the strongest one in all four groups. It shows that, in our case, one- or two-electron de-excitation after quadruple-electron capture may cause other two electrons populated on the higher n shells to be ionized. Like the triple capture, two electrons are likely to be stabilized. We also have found that the double

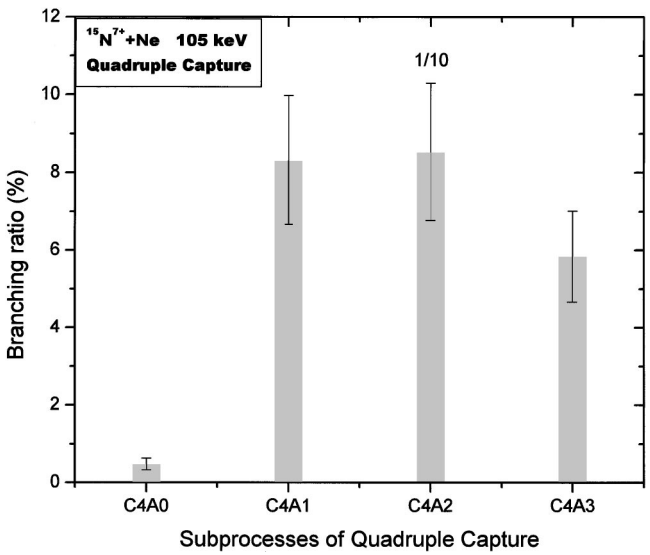

FIG. 8. Measured branching ratios of different subprocesses after quadruple-electron capture for the $^{15}N^{7+}$+Ne system.

Rydberg series of $(2,2,n,n')$ $(n,n'\gg 2)$ and $(2,3,n,n')$ $(n,n'\gg 3)$ are formed whichever decay path is taken after four-electron capture. Those features are very similar to the findings obtained in triple electron capture.

Comparing with triple electron capture, we have found that the quadruple capture is stronger than triple capture, $(C4/C3)=1.33$. The ratio is much greater than SE (0.66) and EOB (0.13). This result implies that the multiple electrons are very likely to be captured in a group, unlike as described by the EOB model, they were captured successively.

According to the N. Selberg, C. Biedermann, and H. Cederquist, semiempirical (SE) scaling laws [12], we have calculated the ratios of between removing two, three and four, and one electron, which are shown in Table VI, along with calculation by EOB. Our measured ratios are also given in Table VI. A qualitatively good agreement has been observed

TABLE V. *Q* values of quadruple electron capture for the N^{7+}+Ne collision.

Configurations	*Q* (eV)
2;2;2;2	274.7038
2;2;2;3	225.0508
2;2;2;4	210.5705
2;2;2;5	204.4368
2;2;2;6	201.7131
2;2;3;3	157.9082
2;2;3;4	140.7303
2;2;4;4	123.6844
2;2;5;5	107.8659
2;3;3;3	81.1171
2;4;4;4	21.2563
3;3;3;3	−0.1588
3;3;4;4	−41.6776
4;4;4;4	−97.4598

TABLE VI. Branching ratios between multiple and single capture for 105 keV $^{15}N^{7+}$+Ne collision.

	DC/SC	C3/SC	C4/SC
SE[a]	0.49	0.29	0.19
EOB[b]	0.71	0.31	0.04
This work	0.69±0.28	0.18±0.07	0.24±0.09

[a]Semiempirical.

[b]Extended over the barrier model.

between our measurement and theoretical data. It seems that SE overestimates C3 and underestimates C4, since we know using SE to estimate SC is not very appropriate, and because at our collision energy, direct single ionization might be of some importance. Therefore, we can only conclude that C3 is very likely to be overestimated by SE. The calculation of EOB also gives a smaller value on (C4/SC), and a larger value on (C3/SC) than our experimental data, but a good agreement on (DC/SC). So, EOB also overestimates C3 and underestimates C4. The difference between our experimental data and EOB may be due to the fact that EOB is an independent electron model: This model has not considered electron-electron correlation, in other words, it ignores the possibility of capturing simultaneously two or more electrons at the same inter-nuclear distance. Of course, the oversimplified description implied in the EOB model could also contribute to the deviation of the prediction from experimental results. In order to explore electron-electron correlation in multiple-electron capture, a further theoretical calculation other than the independent electron model, as well as more sophisticated experiments, are required.

E. Quintuple-electron capture (C5)

For quintuple-electron capture, we only have three processes, which are quintuple-electron capture followed by three-electron autoionization (C5A3), quintuple-electron capture followed by two-electron autoionization (C5A2), and quintuple-electron capture followed by one-electron autoionization (C5A1). We give *Q*-value spectra and populated configurations for these processes in Fig. 9. The corresponding *Q* values of configurations in Fig. 9 are given in Table VII.

From these limited spectra, we find a similar feature as that observed in triple and quadruple capture: two-electron stabilization is easier than three- and four-electron stabilization. The feature that two electrons are most likely to be stabilized has been shown by this experiment through three- to five-electron capture processes. We think the main reason is that, one or two, even three electrons, populate on the Rydberg states after capturing multiple electrons, these Rydberg states could be easily ionized through the de-excitation of one or two electrons.

IV. CONCLUSION

In conclusion, experimental relative cross sections for single-, double-, and multiple-electron capture from $^{15}N^{7+}$+Ne system at 108 keV have been obtained. The single-electron capture results show that an electron could be

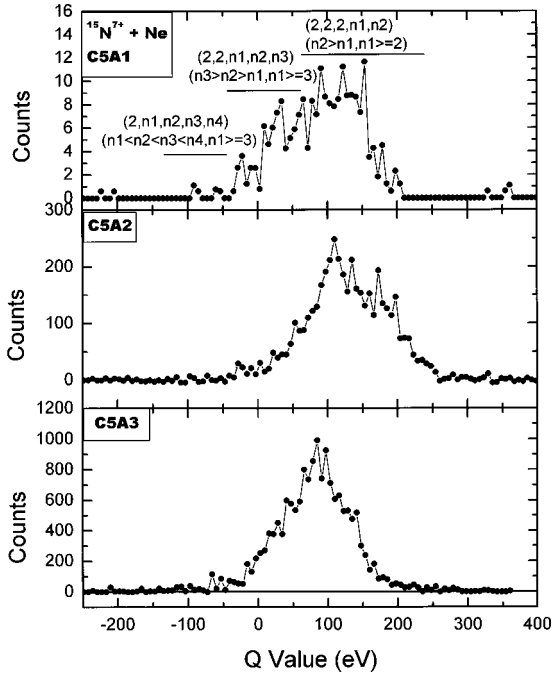

FIG. 9. Measured quintuple-capture *Q*-value spectra for the $^{15}N^{7+}$-Ne system. Different configurations and corresponding *Q* values are given in Table VII.

TABLE VII. *Q* values of quintuple electron capture for the N^{7+}+Ne collision.

Configurations	*Q* (eV)
2,2,2,2,2	206.5169
2,2,2,2,3	170.5886
2,2,2,2,4	158.9355
2,2,2,2,5	154.7074
2,2,2,2,6	142.4282
2,2,2,2,7	141.2432
2,2,2,3,3	108,2600
2,2,2,4,4	85,9526
2,2,2,5,5	76,0680
2,2,2,6,6	70,8195
2,2,3,3,3	55.8681
2,2,3,3,4	46.3137
2,2,3,3,5	41.0713
2,2,3,3,6	38.6518
2,2,3,3,7	37.3184
2,2,3,3,8	33.6546
2,2,3,4,4	26.5185
2,2,3,4,5	21.9317
2,2,3,5,5	16.2195
2,2,4,4,4	11,5836
2,2,4,4,5	5.5503
2,2,4,4,6	3.9212
2,2,4,4,7	2.3851
2,2,5,5,5	−8.3029
2,3,3,3,3	−9.0887

easily captured into the N shell; M shell and O shell take the next priority. Double capture shows that $(3,nl)$ $(n \geqslant 3)$ configurations are mostly populated. However, $(2,nl)$ $(n \geqslant 2)$ have the largest stabilization ratio. Triple-, quadruple-, and quintuple-electron capture show that electrons can populate double Rydberg states and prefer to be doubly stabilized after multiple-electron capture. The result that the quadruple capture is stronger than triple capture, which is different from the prediction of the independent electron model, implies that multiple capture may have strong electron-electron correlation. The over-the-barrier model could still be used to describe multiple-capture processes, however, due to the fact that it ignores the electron-electron correlation and oversimplifies the electron-transfer processes, it could not give precise description for multiple capture.

ACKNOWLEDGMENT

We thank Professor K. B. MacAdam of the University of Kentucky for helpful discussions.

[1] M. Barat and P. Roncin, J. Phys. B **25**, 2205 (1992).
[2] J. Ullrich, R. Moshammer, R. Dömer, O. Jagutzki, V. Mergel, H. Schmidt-Böcking, and L. Spielberger, J. Phys. B **30**, 2917 (1997).
[3] A. Cassimi, S. Duponchel, X. Flechard, P. Jardin, P. Sortais, D. Hennecart, and R. E. Olson, Phys. Rev. Lett. **76**, 3679 (1996).
[4] Hualin Zhang, X. Flechard, A. Cassimi, L. Adoui, F. Fremont, D. Lecler, G. Cremer, L. Guillaume, D. Lelievre, A. Lepoutre, and D. Henecart, Phys. Rev. A **60**, 3694 (1999).
[5] J. H. Posthumus and R. Morgenstern, Phys. Rev. Lett. **68**, 1315 (1992).
[6] R. Ali, C. L. Coke, M. L. A. Raphaelian, and M. Stöckli, Phys. Rev. A **49**, 3586 (1994).
[7] M. L. A. Raphaelian, M. P. Stöckli, W. Wu, and C. L. Cocke, Phys. Rev. A **51**, 1304 (1995).
[8] Serge Martin, Jerome Bernard, Li Chen, Alain Denis, and Jean Desesquelles, Phys. Rev. Lett. **77**, 4306 (1996).
[9] H. Merabet, H. M. Cakmak, E. D. Emons, A. A. Hasan, T. Osipov, R. A. Phaneuf, and R. Ali, Phys. Rev. A **59**, R3158 (1999).
[10] A. A. Hasan, E. D. Emmons, G. Hinojosa, and R. Ali, Phys. Rev. Lett. **83**, 4522 (1999).
[11] E. D. Emmons, A. A. Hasan, and R. Ali, Phys. Rev. A **60**, 4616 (1999).
[12] N. Selberg, C. Biedermann, and H. Cederquist, Phys. Rev. A **54**, 4127 (1996).
[13] N. Selberg, C. Biedermann, and H. Cederquist, Phys. Rev. A **56**, 4623 (1997).
[14] X. Fléchard, Ph.D thesis, Caen University of France, 1999; D. Hennecart, X. Fléchard, F. Frémont, A. Lepoutre, S. Duponchel, L. Adoui, and A. Cassimi, in *Photonic and Atomic collisions*, Proceedings of the 20th International Conference of Electronic and Atomic Collisions (World Scientific, Singapore, 1997), p. 557.
[15] A. Niehaus, J. Phys. B **19**, 2925 (1986).
[16] P. Sortais, Nucl. Instrum. Methods Phys. Res. B **98**, 508 (1995).
[17] L. D. Landau, Phys. Z. Sowjetunion **2**, 46 (1932); C. Zener, Proc. R. Soc. London, Ser. A **137**, 696 (1932).
[18] R. D. Cowan, *The Theory of Atomic Structure and Spectra* (University of California, Berkeley, 1981).
[19] N. Stolterfoht, C. C. Havener, R. A. Phaneuf, J. K. Swenson, S. M. Shafroth, and F. W. Meyer, Phys. Rev. Lett. **57**, 74 (1986).
[20] H. Winter, M. Mack, R. Hoekstra, A. Niehaus, and F. de Heer, Phys. Rev. Lett. **58**, 957 (1987).
[21] H. Laurent, M. Barat, M. N. Gaboriaud, L. Guillemot, and P. Roncin, J. Phys. B **20**, 6581 (1987).